Effects of Protons on the Oxygenation-Linked Subunit Assembly in Human Hemoglobin†

Amy H. Chu,‡ Benjamin W. Turner, and Gary K. Ackers*

ABSTRACT: To investigate the role of protons in the cooperative mechanism of human hemoglobin, the thermodynamic linkage between stepwise oxygen binding and dimer–tetramer assembly was studied over the pH range 7.4–9.5 at 21.5 °C. At each pH, oxygen binding isotherms were measured at a series of protein concentrations. These data were analyzed for microscopic free energies of the constituent reactions according to a model-independent thermodynamic treatment [Ackers, G. K., & Halvorson, H. R. (1974) *Proc. Natl. Acad. Sci. U.S.A. 74*, 4312–4316]. The analysis incorporated equilibrium constants for the assembly of unliganded and fully oxygenated species that were independently determined under identical conditions [Chu, A. H., & Ackers, G. K. (1981) *J. Biol. Chem. 256*, 1199–1205]. From the pH dependencies of the derived equilibrium constants of the linkage system, we have calculated the apparent changes in proton binding that accompany all the reactions of subunit assembly and oxygen binding. The tetramer Bohr effect was also analyzed according to a thermodynamic treatment based on integral relationships between the linked functions. Principal results are as follows: (1) At all pH values, a major fraction of the intersubunit interaction energy, which "pays" for cooperativity in oxygen binding, is "spent" at the first oxygenation step. Changes occur at every pH in the intersubunit contact energy between four stages of oxygenation: unliganded, singly, triply, and fully oxygenated. (2) The *quaternary enhancement* effect, previously found at pH 7.4 over a wide temperature range [Mills, F. C., & Ackers, G. K. (1979) *J. Biol. Chem. 254*, 2881–2887], is manifested at all pH values of this study; oxygen binding affinities of triply liganded tetramers are significantly higher than the mean affinity per heme of the (noncooperative) dimers. (3) Release of Bohr protons by the tetramer is essentially complete after the first three oxygens are bound. Of these protons, 20–25% are released upon binding the first oxygen. (4) Analysis of the composite data confirmed the existence and magnitude of the dimer Bohr effect reported previously. (5) For tetramers, the number of Bohr protons released at each oxygenation step is proportional to the corresponding stepwise change in enthalpy. The heats of proton release account for all the enthalpies of cooperativity in tetramer oxygen binding.

The human hemoglobin molecule changes its affinity for protons and oxygen at each successive oxygenation step. A major goal of hemoglobin research is to understand the molecular mechanism of these coupled self-regulatory processes. Since hemoglobin operates essentially as an equilibrium thermodynamic system in vivo, the problem of delineating its structure–function relationships becomes one of establishing relationships between changes in thermodynamic and structural properties that accompany the molecule's functional cycle of oxygenation–deoxygenation. Detailed knowledge of the relationships between the energetic transitions and functional events (e.g., O_2 binding, proton binding) provides important constraints on all mechanistic theories of hemoglobin action.

The self-regulation properties of hemoglobin are mediated through interactions at the intersubunit contacts of the tetrameric molecule. Subunit dissociation has therefore proven to be a powerful quantitative tool for probing the regulatory energy changes that accompany the molecule's functional cycle. The rationale for this approach is as follows: (1) Interactions within the tetrameric molecule which are responsible for cooperativity can be decoupled by dissociation of the tetramers into noncooperative dimers. (2) The difference between energies of dimer–tetramer assembly at any two stages of oxygenation provides a measure of how much the interaction energy within the tetramer is changed as a result of the oxygen binding. (3) It is these changes in the interaction energy (δ_{4i}) that "pay" for cooperativity in oxygen binding: the free energy of binding at each step (i = 1, 2, 3, and 4) is given by $\Delta G_{4i} = \langle \Delta G \rangle_{4i} + \delta_{4i}$, where $\langle \Delta G \rangle_{4i}$ is the statistical average energy of binding for the isolated subunits ($2\alpha + 2\beta$). Recent work indicates that the energies of interaction (δ_{4i}) arise from structure changes that are mostly localized at the $\alpha^1\beta^2$ intersubunit contact region of the tetramer (Pettigrew et al., 1982). These results reinforce the validity and importance of using subunit dissociation as a quantitative probe in this system.

The tetrameric complex $\alpha_2\beta_2$ dissociates reversibly into two $\alpha^1\beta^1$ dimers, eliminating the intersubunit contact where the major changes in quaternary structure and regulatory energy occur upon ligation (i.e., the $\alpha^1\beta^2$ contact). Dissociation equilibrium constants for unliganded and fully oxygenated molecules differ by as much as 5 orders of magnitude (Ip et al., 1976), providing an exquisitely sensitive probe of the regulatory interactions.

Several years ago, we developed a general approach to the problem of experimentally resolving and interpreting the stepwise changes in oxygenation-linked intersubunit interaction energy by using a combination of subunit dissociation and oxygen binding measurements [for recent reviews, cf. Ackers (1980), Turner et al. (1981)]. This approach was based upon three developments: (1) Theoretical treatment of the thermodynamic linkage problem provided a model-independent framework for analyzing the experimental data (Ackers & Halvorson, 1974; Johnson et al., 1976). (2) Experimental techniques were developed for determining both the set of equilibrium constants for subunit assembly at different stages of oxygenation (Ip et al., 1976; Ip & Ackers, 1977; Ackers

† From the Department of Biology and the McCollum–Pratt Institute, The Johns Hopkins University, Baltimore, Maryland 21218. *Received April 8, 1983; revised manuscript received July 26, 1983.* This work was supported by National Science Foundation Grant PCM 23321 and National Institutes of Health Grant GM24486.

* Address correspondence to this author at the Department of Biology, The Johns Hopkins University, Baltimore, MD 21218.

‡ Present address: Office of Naval Medical Research, Bethesda, MD 20814.

0006-2960/84/0423-0604$01.50/0

et al., 1978) and the degree of oxygen binding at different stages of subunit assembly (Mills et al., 1976). (3) Computational procedures were developed for resolving reliably the thermodynamic constants from these experimental data (Johnson et al., 1976; Johnson & Ackers, 1977).

Initial resolution of the hemoglobin linkage system (Mills et al., 1976; Mills & Ackers, 1979a) established the distribution of intersubunit contact energy changes at each successive oxygenation step for a single set of conditions. In subsequent studies, we have used the same methodology to resolve these interactions as a function of temperature (Mills & Ackers, 1979b) and to relate those results to the ligand-linked assembly properties of isolated subunit chains (Valdes & Ackers, 1977a,b; Mills et al., 1979). That work provided a resolution of the stepwise enthalpic and entropic contributions to the subunit interactions and led to the discovery of *quaternary enhancement*; i.e., the assembly of hemoglobin subunits can generate an increase in the affinity for oxygen (Mills & Ackers, 1979a; Valdes & Ackers, 1978a,b). Using the same methodology as our studies, Riggs and colleagues have resolved the oxygenation-linked subunit assembly properties of the mutant hemoglobin Kansas (β-102 Asp → Asn) (Atha & Riggs, 1976; Atha et al., 1979).

The thermodynamic results obtained to date on the hemoglobin linkage problem have been correlated with structural information by (1) evaluation of noncovalent interactions that may account for the observed patterns of thermodynamic effects (Ackers, 1980; Flanagan et al., 1981), (2) analysis of the data in terms of models for the cooperative mechanism (Ackers & Johnson, 1981; Johnson & Ackers, 1982; Johnson et al., 1984), and (3) studies of thermodynamic coupling between oxygenation and subunit assembly in hemoglobins with structural alterations resulting from mutation or chemical modification (Pettigrew et al., 1982). This work has recently been extended to the analysis of hybrid tetramers of the various $\alpha^1\beta^1$ dimers from mutant and chemically modified hemoglobins (Smith & Ackers, 1983).

Mechanistically significant thermodynamic effects are frequently the result of small differences between much larger energetic terms; e.g., the Gibbs free energies for successive oxygenation steps differ at most by only 3–4 kcal. It is therefore of crucial importance to obtain an extensive and self-consistent set of experimental information on a broad range of properties under precisely comparable conditions. The series of studies referred to above, along with the present work, has been meticulously directed toward this goal. The criteria of self-consistency include not only the use of comparable conditions and hemoglobin preparations but also the use of free-energy balance around thermodynamic cycles, as we shall demonstrate. In this paper, we present results of a detailed study on the pH dependency of the oxygenation-linked subunit assembly in human hemoglobin at a single temperature (21.5 °C) and under the same buffer conditions as those of the previous studies in this series. Comparison of our results with those of other studies, where conditions are sufficiently similar, will be presented under Results and under Discussion.

Theory

In this section, we summarize pertinent aspects of the thermodynamic linkage relationships used in the analysis of data to be presented. We begin (part A) with a brief summary of the theory for oxygenation-linked dimer–tetramer assembly. Next, we consider (part B) the linkage relationships between proton binding and oxygenation which apply to either of the protein species—dimers or tetramers. Part C deals with relationships that arise from the mutual linkage between all three processes—subunit assembly, oxygen binding, and proton binding. The principal symbols used throughout this paper are given in section B of the Appendix.

(A) Linkage between Dimer–Tetramer Association and Oxygen Binding. The equilibrium states of hemoglobin dimers and tetramers are shown in the linkage scheme below, and the free-energy relationships are diagrammed.

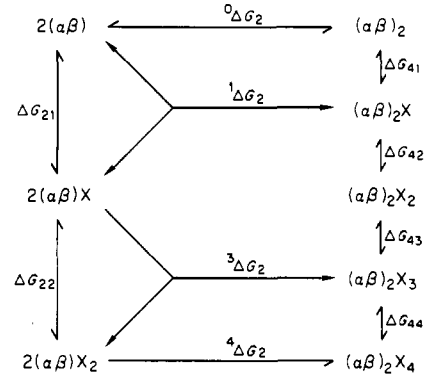

(1)

This linkage scheme indicates the processes under consideration but does not represent balanced chemical reactions. Species designated $(\alpha\beta)_2X_i$ represent hemoglobin tetramers with "i" oxygen molecules bound, and states designated $(\alpha\beta)X_i$ represent the corresponding dimeric species. Each species shown in the linkage scheme is a well-defined average over the many possible microscopic states, as are the corresponding equilibrium constants and free energies. To resolve the equilibria in the linkage scheme, at least seven independent constants must be known. The Adair oxygen binding constants are defined as

$$K_{4i} = \frac{[(\alpha\beta)_2X_i]}{[(\alpha\beta)_2][X]^i} \qquad i = 1, 2, 3, 4 \tag{2}$$

$$K_{2i} = \frac{[(\alpha\beta)X_i]}{[\alpha\beta][X]^i} \qquad i = 1, 2 \tag{3}$$

While the Adair constants are more convenient for defining linkage relationships and binding isotherms, the stepwise sequential constants which define the ligand binding energy at each step are given by

$$k_{4i} = \frac{[(\alpha\beta)_2X_i]}{[(\alpha\beta)_2X_{i-1}][X]} \qquad i = 1, 2, 3, 4 \tag{4}$$

and

$$k_{2i} = \frac{[(\alpha\beta)X_i]}{[(\alpha\beta)X_{i-1}][X]} \qquad i = 1, 2 \tag{5}$$

These binding constants are defined relative to a thermodynamic reference state of 1 mol/L at 21.5 °C, for all reactants and products. The equilibrium constants for formation of tetramers in the various liganded states are

$$^iK_2 = \frac{[(\alpha\beta)_2X_i]}{[(\alpha\beta)X_j][(\alpha\beta)X_k]}$$

$$j + k = i \qquad j, k = 0, 1, 2 \tag{6}$$

The reference state for these assembly reactions is 1 mol/L at 21.5 °C for dimers or tetramers. The oxygen binding function ($\bar{Y}$) for the linkage system may be formulated as

$$\bar{Y} = f_2([P_t], [X])\bar{Y}_2([X]) + f_4([P_t], [X])\bar{Y}_4([X]) \tag{7}$$

Where f_2 and f_4 are respectively the weight fractions of dimeric and tetrameric species at total protein concentration ($[P_t]$)

(molar heme) and oxygen concentration ([X]) (molar O_2). $\bar{Y}_2$ and $\bar{Y}_4$ are dimer and tetramer saturation functions. These depend only upon the oxygen concentration. The saturation function may be expressed in more explicit form as

$$\bar{Y} = \frac{Z_2' + Z_4'(\sqrt{Z_2^2 + 4^0K_2Z_4[P_t]} - Z_2)/(4Z_4)}{Z_2 + \sqrt{Z_2^2 + 4^0K_2Z_4[P_t]}} \quad (8)$$

where

$$Z_2 = 1 + K_{21}[X] + K_{22}[X]^2$$

$$Z_2' = K_{21}[X] + 2K_{22}[X]^2$$

$$Z_4 = 1 + K_{41}[X] + K_{42}[X]^2 + K_{43}[X]^3 + K_{44}[X]^4$$

$$Z_4' = K_{41}[X] + 2K_{42}[X]^2 + 3K_{43}[X]^3 + 4K_{44}[X]^4 \quad (9)$$

Here the six Adair constants for the dimeric and tetrameric species along with $^0K_2$ (the dimer–tetramer association constant for unliganded hemoglobin) comprise the necessary set of independent constants.

This expression illustrates how the presence of the reversible dimer–tetramer equilibrium can produce a marked protein concentration dependence upon the shape and "position" of the observed oxygenation curves. Over the pH range of this study, the unliganded tetramer is more stable than the fully oxygenated tetramer by free energies that range from 3.0 to 6.6 kcal/mol (Chu & Ackers, 1981). At a given protein concentration, as fractional saturation decreases, the contribution to $\bar{Y}$ from the dimeric species ($\bar{Y}_2$) drops nearly to zero. The extent of this change depends upon the values of the constants $^0K_2$ and $^4K_2$ as well as upon the total protein concentration. The manner in which the transition occurs at a given pH is a function of all equilibrium constants of the linkage system.

In principle, a complete set of the parameters described above could be resolved from the protein concentration dependent oxygenation curves alone. However, analysis of simulated data (covering the range of protein concentrations and precision experimentally achievable) has shown that such data are incapable of simultaneously determining all seven of the requisite constants. This limitation results both from the expected random experimental error and from the relationship between the range of protein concentrations and the actual values of the equilibrium constants. In practice, it has been possible to determine independently the values for the subunit association constants ($^0K_2$ and $^4K_2$) in unliganded and fully oxygenated states. Values for these two constants as a function of pH were reported previously (Chu & Ackers, 1981).

The set of undetermined constants is further reduced through use of the *median ligand concentration* (Wyman, 1964) defined by

$$\int_{[X]=0}^{[X]=[\bar{X}]} \bar{Y}\, d\ln[X] = \int_{[X]=[\bar{X}]}^{[X]=\infty} (1 - \bar{Y})\, d\ln[X] \quad (10)$$

The median ligand concentration, $[\bar{X}]$, provides a measure of the free energy of bringing the system from the unliganded state, $\bar{Y} = 0$, to the fully liganded state, $\bar{Y} = 1$. The quantity $\ln[\bar{X}]$ is the centroid of the $\bar{Y}$ vs. $\ln[X]$ isotherm and $[\bar{X}]$ may be determined directly from numerical integration of each experimental oxygenation curve according to the expression

$$[\bar{X}] = \exp\left(\int_{\bar{Y}=0}^{\bar{Y}=1} \ln[X]\, d\bar{Y}\right) \quad (11)$$

The relationship between $[\bar{X}]$ and K_{44} is given by (Johnson et al., 1976)

$$K_{44} = [\bar{X}]^{-4}\left(\frac{1 - {}^4f_2}{1 - {}^0f_2}\right)\exp({}^0f_2 - {}^4f_2) \quad (12)$$

where

$${}^0f_2 = \frac{\sqrt{1 + 4[P_t]^0K_2} - 1}{2[P_t]^0K_2} \quad (13a)$$

$${}^4f_2 = \frac{\sqrt{1 + 4[P_t]^4K_2} - 1}{2[P_t]^4K_2} \quad (13b)$$

Although this determination of K_{44} uses the same oxygenation curve data as the multiparameter saturation curve analysis, calculation of $[\bar{X}]$ is independent of the functional form of $\bar{Y}$ and also of the detailed shape of the oxygenation curve. As a result, correlations between this value for K_{44} and parameters other than $^0K_2$ and $^4K_2$ are effectively decoupled in the numerical analysis of the data. With $^0K_2$, $^4K_2$, and K_{44} determined independently, it is possible to analyze the oxygenation data in various ways to obtain physically meaningful parameters that describe the remainder of the linkage scheme [cf. Johnson et al. (1976)].

(B) Linkage between Proton Binding and Oxygenation of Tetramers or Dimers. The hemoglobin tetramer has approximately 182 titratable sites for protons (Matthew et al., 1979a), and a significant number of these appear to have altered probabilities of proton binding when the molecule is reacted with oxygen [e.g., see Russu et al. (1982, 1983) and Matthew et al. (1979b)]. This phenomenon is known classically as the Bohr effect [cf. Edsall (1972) for a historical account of early work] and has been studied extensively from a variety of viewpoints [also cf. Antonini et al. (1965a), Rossi-Bernardi & Roughton (1967), Chipperfield et al. (1967), Kilmartin et al. (1980), Russu et al. (1983), Rollema et al. (1975), and Matthew et al. (1979a,b)]. Here we are concerned with thermodynamic relationships which correlate the experimental measurements of oxygen binding and proton titration. The treatment described is theoretically applicable to proton binding of oxy and deoxy dimers as well as to the tetramers.

Consider the following thermodynamic cycle:

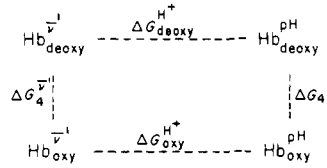

(14)

The species on the left are tetramers in unliganded and fully oxygenated states at a pH where the titration curves coincide with a value $\bar{\nu}'$ (i.e., where no Bohr effect is present). $\Delta G_4^{\bar{\nu}'}$ is the free energy of oxygenating all four sites at this pH. $\Delta G_4^{\bar{\nu}'} = -RT \ln K_{44}$ where K_{44} is the Adair constant at the pH corresponding to $\bar{\nu}'$. The species on the right are tetramers at an arbitrary pH where the titration curves of deoxy- and oxyhemoglobin represent different degrees of saturation with protons, $\bar{\nu}^{pH}_{deoxy}$ and $\bar{\nu}^{pH}_{oxy}$, respectively. ΔG_4 is the free energy of fully oxygenating the tetramers at this pH and includes contributions from (1) reaction of oxygen with the individual subunits, (2) release of Bohr protons from the ionized amino acid side chains and (3) other "structural" effects that accompany oxygen binding (e.g., energies of tertiary and quaternary structure change, solvent interaction terms, interactions with other ions, etc.). $\Delta G^{H^+}_{deoxy}$ is the free energy of protonation as represented by the proton titration curve between the pH

corresponding to $\bar{\nu}'$ and the pH of the right-hand species. This term includes energetic contributions from reaction of protons with amino acid side chains and other structural effects that may accompany the binding of protons to the deoxy tetramer. $\Delta G_{oxy}^{H^+}$ includes similar kinds of energetic contributions from processes that accompany proton binding by the oxygenated molecule.

For the reactions of this thermodynamic cycle, conservation of free energy dictates that

$$\Delta G_4 - \Delta G_4^{\bar{\nu}'} = \Delta G_{oxy}^{H^+} - \Delta G_{deoxy}^{H^+} \equiv \delta\Delta G_{Bohr} \quad (15)$$

The linkage energy, $\delta\Delta G_{Bohr}$, which may be termed the "free energy of the Bohr effect", is manifested identically whether the system is "probed" by oxygen or by protons.

Considering the titration curves that have been obtained for human hemoglobin [e.g., see Antonini et al. (1965a), Rossi-Bernardi et al. (1967), and Rollema et al. (1975)], we may identify $\Delta G_4^{\bar{\nu}'}$ with the free energy of oxygenation at pH 9.5. The experimental values of K_{44} obtained in this study permit us to estimate $\delta\Delta G_{Bohr}$ at several pH values according to the expression on the left side of eq 15. In order to evaluate the correspondence between the linkage free energy $\delta\Delta G_{Bohr}$ calculated from oxygen binding and that reflected by proton titration studies, we may utilize the relationship

$$\Delta G_{oxy}^{H^+} - \Delta G_{deoxy}^{H^+} = RT\int_{[H^+]'}^{[H^+]} (\bar{\nu}_{oxy} - \bar{\nu}_{deoxy})\, d \ln [H^+] \quad (16)$$

where $\bar{\nu}_{oxy}$ and $\bar{\nu}_{deoxy}$ are the fractional saturations with protons for oxy- and deoxyhemoglobin, respectively. $[H^+]'$ is the hydrogen ion activity corresponding to the pH where the two titration curves coincide (i.e., the left side of thermodynamic cycle 14), and $[H^+]$ represents any other pH value. The free-energy correspondence between protonation and oxygenation given by eq 15 and 16 has not, to our knowledge, been previously used in spite of the immense amount of experimental work on the Bohr effect. A derivation of eq 16 is given in section A of the Appendix. This fundamental relationship provides a means to calculate the linkage free energy $\delta\Delta G_{Bohr}$ from direct numerical integration of the difference between the titration curve of unliganded hemoglobin and that of fully oxygenated hemoglobin without any recourse to assumptions regarding the number and nature of the oxygenation-linked ionizable groups, their pKs, etc. The results may then be compared with those obtained from the direct oxygenation measurements at various pH values, according to eq 15.

Equation 16 also leads to the classical linkage relationships for the Bohr effect which are expressed in terms of derivatives (Wyman, 1964). We note that

$$\bar{\nu}_{oxy} = \frac{d \ln Z_{oxy}^{H^+}}{d \ln [H^+]} \quad (17a)$$

$$\bar{\nu}_{deoxy} = \frac{d \ln Z_{deoxy}^{H^+}}{d \ln [H^+]} \quad (17b)$$

where $Z_{oxy}^{H^+}$ and $Z_{deoxy}^{H^+}$ are respectively the binding polynomials of protons for oxygenated and unliganded hemoglobins; e.g., $Z_{oxy}^{H^+} = \sum k_t[H^+]^t$ where k_t is the equilibrium constant for binding t protons. For each state of oxygenation, we consider the entire proton binding curve from $[H^+] = 0$ up to some designated pH. Substituting the above expression for $\bar{\nu}_{oxy}$ and $\bar{\nu}_{deoxy}$ into eq 16, we note from eq 15 that the left side will equal $RT \ln (K_{44}/K_{44}^0)$ where K_{44}^0 is the equilibrium constant for binding four oxygens in the absence of any proton binding. Then eq 16 leads to[1]

$$K_{44} = K_{44}^0 \frac{Z_{oxy}^{H^+}}{Z_{deoxy}^{H^+}} \quad (18)$$

Taking derivatives

$$\frac{d \ln K_{44}}{d \ln [H^+]} = \frac{d \ln K_{44}^0}{d \ln [H^+]} + \bar{\nu}_{oxy} - \bar{\nu}_{deoxy} \quad (19)$$

Provided the protons have no concentration-dependent effect other than binding, so that $d \ln K_{44}^0/d \ln [H^+] = 0$, eq 19 becomes the well-known Wyman relationship:

$$\frac{d \log K_{44}}{d\,pH} = \Delta\bar{\nu}_4 \quad (20a)$$

For dimers, a similar derivation leads to

$$\frac{d \log K_{22}}{d\,pH} = \Delta\bar{\nu}_2 \quad (20b)$$

where $\Delta\bar{\nu}_4$ and $\Delta\bar{\nu}_2$ are the net moles of protons released upon complete oxygenation of tetramers and dimers, respectively.

(C) Mutual Effects of Dimer–Tetramer Association, Proton Binding, and Oxygenation. The coupling between the assembly of tetramers having i oxygens bound (eq 1) and the binding of protons is expressed by the relationship

$$^iK_2 = {}^iK_2^0 \frac{Z_4^{H^+}}{Z_2^{H^+}(Z_2^{H^+})'} \quad (21)$$

where $^iK_2^0$ is the dimer–tetramer assembly constant when no protons are bound, $Z_4^{H^+}$ is the binding polynomial for protons binding to the tetramer, and $Z_2^{H^+}$ and $(Z_2^{H^+})'$ are the proton binding polynomials of the constituent dimers from which the tetramer is assembled. The binding polynomials used here, and also in eq 9, 17, and 18, are related to the grand canonical partition function [cf. Johnson & Ackers (1982)].

From a complete resolution of the linkage scheme (eq 1) carried out at a series of pH values, we can estimate the net release, $^i\Delta\bar{\nu}_2$, of bound protons that results from subunit assembly:

$$^i\Delta\bar{\nu}_2 = \frac{d \log {}^iK_2}{d\,pH} \quad (22)$$

which follows from eq 21 provided there are no additional effects of protons other than binding.

We have used this general type of relationship to estimate the changes in the number of protons for all reactions of the linkage scheme.

Additional use can be made of the combined linkage between subunit assembly, proton binding, and oxygenation to estimate the proton titration curves of dimers. For deoxyhemoglobin, eq 22 becomes

[1] If the ionizable groups are all independent, the binding polynomials of eq 18 can be factored into binomial expansions, so that

$$K_{44} = K_{44}^0 \frac{\prod_i\{1 + k_i^{oxy}[H^+]^i\}}{\prod_i\{1 + k_i^{deoxy}[H^+]^i\}}$$

In this case, the free-energy contribution to K_{44} due to the binding of protons is

$$\delta\Delta G_{Bohr} = RT \ln \frac{\prod_i\{1 + k_i^{oxy}[H^+]^i\}}{\prod_i\{1 + k_i^{deoxy}[H^+]^i\}}$$

It should be remembered that this proton-linked contribution includes all energy changes of the system that accompany the proton binding, not just the energy of ionization of the local proton binding groups.

$$\frac{d \ln {}^0K_2}{d \ln [H^+]} = {}^0\bar{\nu}_4 - 2{}^0\bar{\nu}_2 \quad (23a)$$

where ${}^0\bar{\nu}_4$ and ${}^0\bar{\nu}_2$ are the proton binding isotherms for deoxy tetramers and deoxy dimers, respectively. Combining values of ${}^0K_2$ vs. pH with an independently determined proton titration curve of tetramers, we can estimate values of ${}^0\bar{\nu}_2$ at a series of pH values. Similarly, for conditions where all species are saturated with oxygen

$$\frac{d \ln {}^4K_2}{d \ln [H^+]} = {}^4\bar{\nu}_4 - 2{}^2\bar{\nu}_2 \quad (23b)$$

and we may estimate values of the proton titration curve for oxy dimers, ${}^2\bar{\nu}_2$ by combining independent results for ${}^4K_2$ vs. pH with those for proton titration of oxygenated tetramers, i.e., ${}^4\bar{\nu}_4$ vs. pH.

Materials and Methods

Oxygen saturation curves were measured by using techniques adapted from the method of Imai et al. (1970). In this method, absorbance changes at single wavelengths determine the fractional oxygen saturation of a sample while a polarographic electrode monitors the corresponding free oxygen concentration in the solution. Appropriate mixtures of oxygen and nitrogen pass over the stirred protein solution. A smoothly varying oxygen concentration and a corresponding extent of saturation are generated from fully oxygenated to completely deoxygenated conditions and back. Simultaneous recording of the data on an X–Y plotter produces a continuous oxygen saturation curve. Adaptation of this method for successful studies of protein concentration dependent oxygen binding has evolved in our laboratory into a set of highly specific procedures. Here we present a description of these procedures at a level of detail necessary for reproducing the results obtained in this study. This description extends but does not duplicate the earlier accounts (Mills et al., 1976, 1979; Mills & Ackers, 1979a,b).

A thermostated stainless-steel cell, similar to that of Imai (1973), was equipped with an oxygen electrode, a thermistor temperature probe, and provisions for stirring the sample and passing gas mixtures over the sample surface. The cell was mounted in the Cary 118C spectrophotometer. The electrode (Beckman 39065) was prepared with a thin Teflon membrane (10 μm), a gift of the late Dr. W. B. Elliot, Department of Biochemistry, State University of New York, Buffalo. The polarization voltage from a mercury cell was adjusted to 800 mV by a potentiometer in a voltage divider circuit. A Keithly 150B microvolt ammeter provided amplification and voltage conversion of the electrode current signal. Analog signals corresponding to oxygen tension and absorbance changes were simultaneously recorded on an Esterline Angus 2417TB X–Y recorder. Temperature control was maintained through the use of an external thermostated circulator (Lauda Brinkmann K2/R) and monitored such that sample temperature did not vary by more than ±0.02 °C during the course of an experiment. Gas mixtures were prepared by using a manifold with rotameter flow indicators from a variety of oxygen–nitrogen mixtures and prepurified nitrogen (Linde). Carefully thermostated hydrators filled with actual sample buffer prevent hydration or evaporation from the sample during an experiment.

System performance characteristics were monitored on a periodic basis. Photometric linearity (to 0.005 absorbance unit at absorbances up to 2.0) was tested by measuring absorbances of weighed dilutions of a standard solution of chromate (Haupt, 1952). Electrode readings for a series of calibrated O_2–N_2 mixtures (from 100% O_2 to 0.03% O_2) provided a test of linearity in the oxygen electrode system. Thermistor probes were calibrated against a mercury thermometer traceable to U.S. National Bureau of Standards certification.

Procedure for Oxygenation Experiments. First the nitrogen end-point and the starting gas mixture end-point readings were calibrated from the oxygen electrode system. Approximately 5 mL of sample was placed in the cell. After equilibration to the appropriate temperature and gas mixture was allowed, and only if the sample absorbance was constant, the deoxygenation process was begun by flowing an O_2–N_2 mixture over the surface of the stirred sample. The gas mixtures were designed to maintain a rate of change in oxygen saturation which could be accurately followed by the oxygen electrode system. Only for the higher protein concentration did release of oxygen from the hemoglobin solutions become slow enough to allow immediate use of pure nitrogen in deoxygenation. Experiments performed at pH 8.5 and above, where oxygen affinity is significantly higher, were begun with the sample equilibrated against 3% O_2 mixtures. Experiments at other pH values were equilibrated with 21% O_2 mixtures to begin near 100% oxygen saturation. After the fully deoxygenated point was reached, reoxygenation was initiated through careful introduction of oxygen-containing mixtures, again maintaining the time rate of change of oxygen tension to within accuracy limits of the electrode. The total time required for either deoxygenation or reoxygenation varied between 1 and 2 h depending on sample concentration and pH. In addition to reproducibility between deoxygenation and reoxygenation curves, a further check on the stability of the sample throughout the experiment was available through the collection of visible spectra before and after the experiment.

Since the experiments were carried out over several orders of magnitude in protein concentration, it was necessary to use multiple wavelengths to obtain workable full-scale absorbance changes in going from oxygenated to deoxygenated samples. For all wavelengths used, the slit width was adjusted to give a 1-nm band-pass. Linearity of absorbance changes with oxygen saturation has been demonstrated (Mills et al., 1976).

Preparations. The major component of normal human hemoglobin, (Hb A_0), was isolated from the blood of nonsmokers (minimizing carbon monoxide bound hemoglobin levels) by the method of Williams & Tsay (1973). The central feature of this method is the use of DEAE-Sephadex ion-exchange chromatography to separate Hb A_0 from the minor components (fetal and glycosylated hemoglobins) and to remove all organic phosphates. Immediately after preparation, the hemoglobin (3–5 mM heme) was frozen rapidly in small droplets in liquid N_2 and stored in liquid N_2 until use. This method of storage ensures stability of samples for virtually indefinite periods of time, as demonstrated in this study (see Results).

Hemoglobins were tested for purity by polyacrylamide gel electrophoresis [tris(hydroxymethyl)aminomethane (Tris)–borate–ethylenediaminetetraacetic acid (EDTA) buffer, pH 8.4] and disc gel isoelectric focusing (LKB ampholytes range, pH 6–8) and found to migrate as a single band in both cases. The preparations were checked for organic phosphates by the method of Ames & Dubin (1960) and found to contain no phosphates to within resolution of the method—5 phosphate molecules per 100 hemoglobin tetramers.

Concentrations of frozen stock solutions were determined by conversion to the cyanomet form using $KFe(CN)_6$ and KCN and using the standard extinction coefficient of 11.0

absorbance units per millimolar heme at 540 nm (van Assendelft, 1975). The fraction of methemoglobin present was determined through an adaptation of the method of Evelyn & Malloy (1938). In this method, a sample is divided into two parts, and one is totally converted to the met form through the addition of $KFe(CN)_6$ for use as a reference. Absorbance changes of both samples are monitored upon the addition of KCN at 630 nm or other wavelengths sensitive to the spectral differences of met- vs. cyanomethemoglobin. The relative fraction of methemoglobin in the original sample is then calculated by

$$F_{\text{met-Hb}} = \frac{\Delta A}{\Delta A_{\text{ref}}}$$

where ΔA is the absorbance change of the test sample after adding KCN and ΔA_{ref} is the corresponding change of the 100% methemoglobin sample. Since this method incorporates its own standard, no particular set of extinction coefficients is needed.

Preparation of Samples for Oxygenation Experiments. Before each experiment, a small quantity of frozen hemoglobin stock was thawed. Except for concentrations above 10^{-4} M heme, a portion of the stock solution was diluted into the experimental buffer and the concentration of that sample calculated from the dilution factor. In order to ensure that the sample is in the correct buffer, higher concentration samples were prepared by passing the stock solution through a G-25 Sephadex column equilibrated with the experimental buffer and then making the necessary dilution. The concentrations of these solutions were then determined spectrophotometrically by using extinction coefficients determined in the course of these studies, again referenced to the cyanomethemoglobin standard extinction coefficient at 540 nm (van Assendelft & Zijlstra, 1975). The fraction of methemoglobin in samples prior to the experiment was always less than 0.5%. In order to maintain low met-Hb levels during experiments, an enzymatic reduction system (Hayashi et al., 1973) was added to all samples. The components were stored in stock solution in a fashion described in Mills et al. (1976), but for the system to be effective over the entire pH range of this study, sample concentrations of all components were doubled. Controls verifying that the reductase system does not affect the oxygenation properties of the system under these buffer conditions have been described (Mills et al., 1976).

Of the reductase system components, glucose 6-phosphate, glucose-6-phosphate dehydrogenase, and catalase were obtained from Calbiochem. The remainder, NADP, ferredoxin–NADP reductase, and ferredoxin, were obtained from Sigma and were the same type as described previously (Mills et al., 1976).

Buffer consisted of 0.1 M Tris (pH 7.4, 8.0, and 8.5) or 0.1 M glycine (pH 8.95 and 9.5), 0.1 M NaCl, and 1.0 mM Na_2EDTA, titrated to the correct pH with concentrated HCl (total Cl^- concentrations were close to 0.18 M). Trizma base, glycine, and Na_2EDTA were from Sigma. Deionized water (Hydro-Services) was used to make up the buffers.

Methods of Oxygenation Curve Analysis. For those curves satisfying the criterion of reproducibility between the deoxygenation and reoxygenation curves, numerical values for the x and y coordinates were recorded manually. On each isotherm, 50–70 points were sampled at approximately equal steps in the degree of saturation. Data from deoxygenation curves only were used in the analyses of this study to minimize contributions of any progressive oxidation or protein denaturation during an experiment. Preliminary determinations of oxygenation curve end points were obtained by extrapolation of absorbance vs. $1/pO_2$ to infinite oxygen tension for 100% saturation and against pO_2 to the calibrated N_2 end point for 0% saturation. In both cases, only data from within 5% of each end were used in the extrapolation procedure, and a first- or second-order polynomial least-squares algorithm was employed.

After absorbance values were converted to fractional saturation, median concentrations for each curve were determined by numerical integration of eq 11. The algorithm for performing the integration combines Lagrange interpolation and Simpson's rule integration techniques. Individual values of K_{44} as determined by each curve were calculated by using eq 12. Self-consistency among K_{44} values at a given pH then served as the next criterion for selecting oxygenation curves for further analysis.

For analysis of oxygenation data in terms of the fundamental saturation function given by eq 8, the set of seven independent parameters chosen were ${}^0K_2$, ${}^4K_2$, K_{44}, log k_{43}, ${}^0K_2/{}^1K_2$, ${}^3K_2/{}^4K_2$, and $K_{\text{coop}\,2}$. $K_{\text{coop}\,2} = K_{21}/[2(K_{22})^{1/2}]$ and is a measure of dimer cooperativity—$K_{\text{coop}\,2} = 1$ when the dimer binds oxygen noncooperatively. Use of this parameter set allows direct incorporation of independently determined values for ${}^0K_2$ and ${}^4K_2$ and median determinations of K_{44}. The remaining set of parameters then represents a tractable fitting problem (Johnson et al., 1976).

A sophisticated nonlinear least-squares parameter estimation program was employed for the analysis of all oxygenation data (Johnson et al., 1976; Turner et al., 1981). Best-fit parameter values corresponding to a minimum in variance are found by using a modified Gauss–Newton procedure. The program reports pairwise cross-correlation between "fitting parameters" at the minimum. Differences between data and the "fitted" curves are plotted against oxygen concentration and extent of saturation. N-Dimensional parameter space is mapped out to determine the worst case joint confidence intervals for fitted parameters. The confidence limits are also propagated through calculations of all other linkage parameters, generating a complete set of parameters and reliable confidence limits (confidence limits reported in this paper correspond to approximately 1 standard deviation). All of these features are used in evaluating the "goodness of fit" and reliability of a particular set of results. The algorithm employed and the significance of these particular methods to this problem have been discussed extensively elsewhere (Turner et al., 1981; Mills et al., 1976; Johnson et al., 1976).

Each curve selected was first analyzed individually by using up to 12 different combinations of log k_{43}, ${}^0K_2/{}^1K_2$, ${}^3K_2/{}^4K_2$, K_{44}, and the two saturation end points as fitting parameters. $K_{\text{coop}\,2}$ was fixed at unity, and the appropriate values for ${}^0K_2$ and ${}^4K_2$ were chosen for each pH. New median oxygen concentrations and corresponding K_{44} values were calculated for any curve whose end points differed from the previous extrapolations by more than 0.1%. If one or more of these estimated parameters were physically unrealistic, the individual curve was eliminated from further treatment. The goal at this stage was to find, for each pH, a set of curves with consistent families of values for the linkage scheme parameters. The sets selected on this basis were then fitted simultaneously. Individual curves that made a distinctly nonrandom contribution to the residuals of a set were removed, and the analysis was repeated with various combinations of parameters as fitting variables. This process produced one or more sets of free energies describing the linkage scheme at each pH studied. At some pH values, the sets of curves were exclusive. At others, the different self-consistent sets contained curves that

appear in two or more sets. The tables of Gibbs free-energy values discussed under Results were obtained by averaging the determined free energies for all sets at that pH. Confidence limits reported are the worst of either (a) the standard error for the average or (b) the widest confidence limits of a single set's determination.

Throughout the analysis, oxygenation curve data were equally weighted. Within any one data set's conditions, instrumental uncertainty is roughly constant. While systematic trends dominate any one curve's residuals, the distributions of residuals for complete data sets are all roughly Gaussian and do not exhibit any consistent correlations with independent or dependent variables. These findings lead us to believe that it is inappropriate to employ any ad hoc weighting functions such as have been advocated by Imai (1981).

The tables of proton release discussed under Results represent numerical evaluation of the following derivative relationship for each corresponding reaction:

$$\Delta\bar{\nu} = \frac{\mathrm{d}\ln K}{\mathrm{d}\ln [\mathrm{H}^+]} = \frac{1}{RT\ln 10}\frac{\mathrm{d}(\Delta G)}{\mathrm{d}(\mathrm{pH})}$$

There are a variety of numerical methods for estimating derivatives of functions from tabulated values. Procedures based upon extensions of interpolating algorithms (e.g., Lagrange differentiation formulas) are best suited for precise, noise-free function values. In these cases, errors in the computation of the derivative arise predominantly from the spacing of the data. To deal with more typical data having uncertainty in parameter values and to accommodate multiple determinations, it is convenient to fit the data to an arbitrary smooth function and evaluate the derivatives from this. The choice of a particular function requires that it match the trends of the data without exaggeration of shape. In this study, we explored polynomials, ratios of polynomials, and sums of exponentials for use as possible smoothing functions. The simplest function satisfactory for calculating derivatives from our free-energy values was an unweighted second-order polynomial [$\Delta G = a + b(\mathrm{pH}) + c(\mathrm{pH})^2$] expressing free energies in terms of pH. The parameter values were taken directly from the original analyses (as shown in the figures) to avoid introducing unnecessary bias which would result from fitting the averaged values of the free energies (cited in the tables). Coefficients were recalculated at each pH, using that point as a new origin (i.e., $x = \mathrm{pH} - \mathrm{pH}_0$) in the least-squares fit. The first derivative and an estimate of the error in its determination thus corresponded to the linear (or first-order) coefficient and its standard error.

Results

A total of 95 new oxygenation curves were measured in this study. Over half of these survived the various criteria for acceptability. The quality and reproducibility of the new curves were similar to those of the preceding work (Mills et al., 1976, 1979; Mills & Ackers, 1979a,b). Analyses of the new data at pH 7.4 matched those of previous sets to within the same consistency as the curves within any set. One curve in the new set was obtained by using a sample from the same hemoglobin preparation employed in a previous study (Mills & Ackers, 1979a), stored in liquid nitrogen since 1978. The new measurements on this preparation yielded results identical with those obtained 3 years earlier. Given this degree of reproducibility, four of the previously obtained sets of data for pH 7.4, 21.5 °C, were included in the present study. In combination, 62 oxygenation curves were incorporated in the analyses. Characteristics of the various data sets are summarized in Table I. Numerical values for these oxygenation curves are provided in the supplementary material (see paragraph at end of paper regarding supplementary material). For each pH, except pH 9.5, the data were divided into several self-consistent sets of curves, as described in the previous section.

Table I: Characteristics of the Various Data Sets

pH	no. of sets	no. of curves	av variance	concn (μM heme) lowest	highest
7.4	5	19	1.70×10^{-5}	4.5	382
8.0	2	9	1.64×10^{-5}	3.1	120
8.5	4	14	3.16×10^{-5}	2.0	85
8.95	4	14	4.45×10^{-5}	1.7	79
9.5	1	6	1.61×10^{-5}	2.3	25

Table II: pH Dependence of Parameters for Fully Oxygenating Tetramers and Dimers

(A) Free Energies of Oxygenation

pH	ΔG_4 (kcal/4 mol of oxygen bound)	ΔG_2 (kcal/2 mol of oxygen bound)
7.4	−27.09 ± 0.05	−16.69 ± 0.2
8.0	−28.61 ± 0.09	−16.84 ± 0.2
8.5	−29.84 ± 0.1	−16.93 ± 0.2
8.95	−29.80 ± 0.2	−16.54 ± 0.4
9.5	−30.19 ± 0.2	−16.65 ± 0.2

(B) Number of Protons Released upon Oxygenation

pH	$\Delta\bar{\nu}_4$ (protons released per four O_2 bound)	$\Delta\bar{\nu}_2$ (protons released per four O_2 bound)
7.4	2.32 ± 0.19	0.22 ± 0.12
8.0	1.61 ± 0.09	0.07 ± 0.05
8.5	1.02 ± 0.07	−0.05 ± 0.04
8.95	0.49 ± 0.14	−0.16 ± 0.09
9.5	0	

Multiple saturation curves obtained at constant protein concentration virtually overlay one another. The method of analysis does not require that data be obtained over a wide range of protein concentrations, but the information content is increased when dimeric species contribute appreciably to the saturation curves. The data analyzed in this study included curves from the lowest concentrations experimentally feasible (1–2 μM heme) and ranged from 10- to 100-fold higher (see Table I). Gibbs free energies resolved from these data are given in Tables II, III, and IV. The values listed are averages over results from the data sets at each pH. For determining the pH dependence of the linkage parameters, however, we used the full set of free energies.

The data reflect contributions of high-affinity dimeric species to the oxygen saturation curves. At each pH, the shape and overall oxygen affinity exhibit a distinct dependence upon hemoglobin concentration. This is illustrated in Figure 1A, showing a subset of the curves at pH 8.5. The complete set consisted of 14 curves, covering a 40-fold range in concentration and including approximately 900 data points. For the sake of clarity, data points of only four distinct protein concentrations are shown together with their fitted curves. The residuals shown in Figure 1B (differences between data points and fitted curves) represent the full data set.

(A) Linkage Properties for Total Oxygenation of Tetramers and Dimers. (1) pH Dependence of Gibbs Energies. Gibbs free energies for complete oxygenation of tetramers ($\Delta G_4 = -RT\ln K_{44}$) were calculated from median oxygen concentrations of individual curves and averaged. The resulting values were also confirmed through analysis for K_{44} values in the detailed fitting process. Binding energies for fully ligating dimers ($\Delta G_2 = -RT\ln K_{22}$) were evaluated at each pH from

Table III: pH Dependence of Microscopic Free Energies of the Linkage System

(A) Dimer-Tetramer Association as a Function of Oxygenation

pH	$^0\Delta G_2$ (kcal/mol)	$^1\Delta G'_2$ (kcal/mol)	$^3\Delta G'_2$ (kcal/mol)	$^4\Delta G_2$ (kcal/mol)
7.4	−14.35 ± 0.1	−11.48 ± 0.18	7.21 ± 0.39	−8.05 ± 0.1
8.0	−13.99 ± 0.1	−11.41 ± 0.1	−8.15 ± 0.18	−8.93 ± 0.1
8.5	−13.27 ± 0.1	−10.85 ± 0.12	−8.35 ± 0.19	−9.25 ± 0.1
8.95	−12.35 ± 0.2	−10.11 ± 0.18	−8.08 ± 0.3	−9.07 ± 0.1
9.5	−11.69 ± 0.1	−9.36 ± 0.08	−7.71 ± 0.1	−8.58 ± 0.1

(B) Intersubunit Contact Energy Changes

pH	$\delta\Delta G'_{01}$ (kcal)	$\delta\Delta G'_{13}$ (kcal)	$\delta\Delta G'_{34}$ (kcal)	$\delta\Delta G_{04}$ (kcal)
7.4	−2.91 ± 0.12	−4.8 ± 0.36	+0.83 ± 0.3	−6.3 ± 0.2
8.0	−2.58 ± 0.09	−3.26 ± 0.27	+0.78 ± 0.18	−5.1 ± 0.1
8.5	−2.41 ± 0.12	−2.51 ± 0.3	+0.9 ± 0.19	−4.0 ± 0.2
8.95	−2.24 ± 0.12	−2.04 ± 0.3	+1.01 ± 0.24	−3.3 ± 0.3
9.5	−2.33 ± 0.08	−1.65 ± 0.18	+0.87 ± 0.11	−3.1 ± 0.2

(C) Free Energies for Successive Tetramer Oxygenation Steps

pH	$\Delta G'_{41}$ (kcal/mol of O_2)	$\Delta G'_{42}$ (kcal/mol of O_2)	$\Delta G'_{43}$ (kcal/mol of O_2)	ΔG_{44} (kcal/mol of O_2)
7.4	−5.43 ± 0.11	−5.54 ± 1.3	−6.96 ± 1.1	−9.16 ± 0.35
8.0	−5.85 ± 0.07	−5.42 ± 1.2	−8.16 ± 1.35	−9.48 ± 0.60
8.5	−6.06 ± 0.13	−6.66 ± 0.6	−7.77 ± 0.9	−9.36 ± 0.53
8.95	−6.04 ± 0.13	−6.61 ± 0.55	−7.89 ± 1.2	−9.26 ± 0.3
9.5	−6.0 ± 0.07	−6.99 ± 0.85	−8.81 ± 0.85	−9.19 ± 0.11

(D) Combined Oxygenation Energies for the Intermediate Steps

pH	$\Delta G'_{4(2+3)}$ (kcal/2 mol of O_2)
7.4	−12.50 ± 0.4
8.0	−13.57 ± 0.35
8.5	−14.41 ± 0.3
8.95	−14.5 ± 0.25
9.5	−15.0 ± 0.17

Table IV: Proton Release and Absorption for the Microscopic Steps of the Linkage System

(A) Protons Released upon Assembly vs. Ligation State of Tetramer

pH	$^0\Delta\bar{\nu}_2$	$^1\Delta\bar{\nu}_2$	$^3\Delta\bar{\nu}_2$	$^4\Delta\bar{\nu}_2$
7.4	−0.62 ± 0.07	−0.06 ± 0.13	+1.39 ± 0.22	+0.87 ± 0.11
8.0	−0.83 ± 0.04	−0.49 ± 0.06	+0.66 ± 0.09	+0.48 ± 0.07
8.5	−1.0 ± 0.06	−0.85 ± 0.05	+0.05 ± 0.09	+0.15 ± 0.09
8.95	−1.16 ± 0.09	−1.17 ± 0.11	−0.49 ± 0.18	−0.14 ± 0.14

(B) Bohr Protons Released upon Stepwise Oxygenation

pH	$\Delta\bar{\nu}_{41}$	$\Delta\bar{\nu}_{4(2+3)}$	$\Delta\bar{\nu}_{44}$
7.4	0.64 ± 0.07	1.62 ± 0.27	0.05 ± 0.06
8.0	0.38 ± 0.03	1.16 ± 0.12	0.05 ± 0.06
8.5	0.16 ± 0.03	0.78 ± 0.11	0.05 ± 0.06
8.95	−0.03 ± 0.06	0.44 ± 0.23	0.05 ± 0.06

values of ΔG_4 and the independently determined subunit assembly energies $^0\Delta G_2$ and $^4\Delta G_2$ (Chu & Ackers, 1981):

$$\Delta G_2 = \tfrac{1}{2}(\Delta G_4 + {}^0\Delta G_2 - {}^4\Delta G_2) \quad (24)$$

Averaged values for ΔG_4 and ΔG_2 appear in Table II, section A.

(*2*) *Magnitudes of Bohr Effects for Tetramers and Dimers.* Both tetramers and dimers exhibited a marked pH dependence in their oxygenation curves. This is illustrated in Figure 2 which shows a set of these individual species curves as reconstructed from the resolved oxygen binding constants K_{4i} and K_{2i}. The numbers of protons released upon complete oxygenation of tetramers ($\Delta\bar{\nu}_4$) and dimers ($\Delta\bar{\nu}_2$) are listed in section B of Table II. Values of $\Delta\bar{\nu}_4$ were not determined for pH 9.5 since, with only a single data set, confidence limits were not acceptable. As shown in Figure 3, the $\Delta\bar{\nu}_4$ values are very similar to literature values from studies performed under

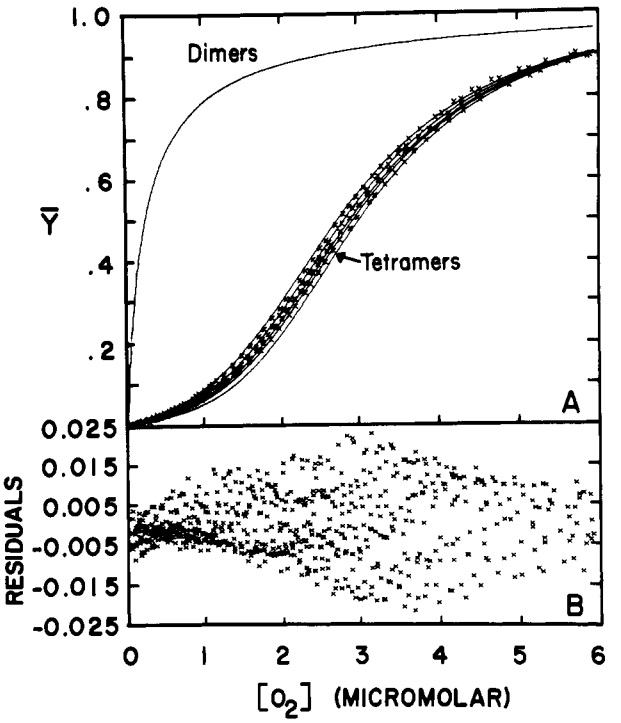

FIGURE 1: Oxygenation curves at pH 8.5 as a function of hemoglobin concentration. (A) Of the 14 curves obtained in this data set, 4 are shown. (Other conditions: 0.1 M Tris-HCl, 0.1 mM NaCl, and 1 mM Na_2EDTA, 21.5 °C.) Solid lines through the data points at each hemoglobin concentration were calculated from eq 8 by using the equilibrium constants resolved from the simultaneous least-squares fit to the composite for all 14 binding curves. Solid curves for dimeric and tetrameric species were calculated from the resolved binding constant. The data shown are for protein concentrations (left to right) of 2.2, 4.6, 13, and 31 μM. (B) Residuals of the least-squares fits, showing the data points for all 14 binding curves of the pH 8.5 data set.

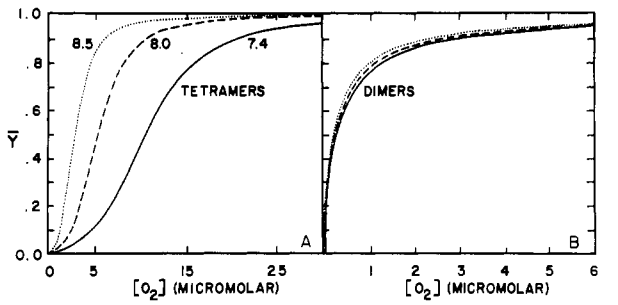

FIGURE 2: pH dependence of tetrameric and dimeric oxygenation curves, resolved from the protein concentration dependent binding curves at each of the pH values.

comparable conditions [Antonini et al., 1965a; cf. also Rossi-Bernardi & Roughton (1967) and Rollema et al. (1975)]. At pH 9.5, the value of $\Delta\bar{\nu}_4$ may be estimated as 0 ± 0.05 from the data of Antonini et al. (1965a). The data of Antonini et al. and of Rossi-Bernardi & Roughton (1967) bear close correspondence to those of the present study in regard to the thermodynamic properties derivable from the difference titration curves of deoxy and oxy tetramers, as shown in Figure 3 and (3) below.

Analysis of the concentration-dependent oxygenation curves also confirmed the magnitude of the *dimer Bohr effect* originally calculated on the basis of conservation of numbers of bound protons around the overall cycle of the linkage scheme (Chu & Ackers, 1981). Figure 3 shows the dimer Bohr effect as a function of pH.

(*3*) *Free Energy of the Tetramer Bohr Effect.* Table V shows the linkage free energy $\delta\Delta G_{Bohr}$ as determined at various

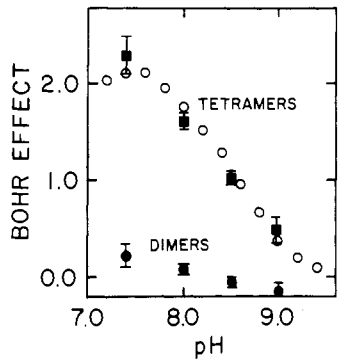

FIGURE 3: Changes in proton binding upon complete oxygenation of tetramers and dimers. Solid points were calculated from the pH dependencies of the equilibrium constants K_{44} and K_{22} by using eq 20. Tetrameric values are the number of protons released upon binding four oxygens; dimeric values are for binding two oxygens. Open circles are from the direct proton titration data of Antonini et al. (1965a,b) at 20 °C, 0.25 M KCl.

Table V: Linkage Free Energy of the Bohr Effect

	$\delta\Delta G_{Bohr}$		
		from proton titration	
pH	from O_2 binding data of this study	data of Antonini et al. (1965a,b)	data of Rollema et al. (1975)
9.5	0	0.01	0.0
9.0	0.4 ± 0.3	0.15	0.0
8.5	0.4 ± 0.2	0.67	0.24
8.0	1.6 ± 0.2	1.63	0.90
7.4	3.1 ± 0.2	3.24	2.25

pH values from the results of this study by using the value of ΔG_4 at pH 9.5 for ΔG_4^{ν} in eq 15. We see that, in going from pH 9.5 (where Bohr proton release is absent) to pH 7.4, the free energy of tetramer oxygenation is reduced by 3.1 kcal. In order to test our results against the linkage relationships of eq 15, we calculated the difference free energy (oxy minus deoxy) of proton binding over the same pH range by using the data of Antonini et al. (1965a). Figure 4 shows a plot of the difference function $\bar{\nu}_{deoxy} - \bar{\nu}_{oxy}$ taken from the data set at 20 °C, 0.25 M KCl (Antonini et al., 1965a). Numerical integration of the difference function was performed according to eq 16 to yield the values of linkage free energy, $\delta\Delta G_{Bohr}$, corresponding to the same pH values as the ΔG_4 values determined in this study. Comparison of the $\delta\Delta G_{Bohr}$ values is made in Table V. The corresponding energies obtained by independent methods are seen to be in excellent agreement.

This method of establishing on energetic grounds the linkage between protonation and oxygenation does not suffer from the uncertainties of applying derivative relationships like eq 20 to experimental data points that exhibit both scatter and functional variation. The close correlation obtained between the linked functions in their integral form adds confidence to the overall accuracy of the experimental results obtained in this study. Moreover, these results provide support for the assumption that d ln K_{44}^0/d ln $[H^+] = 0$ in eq 19, so that the derivative linkage relationship for $\Delta\bar{\nu}_4$ is valid. For comparison, we also show (Table V) values of $\delta\Delta G_{Bohr}$ obtained by integrating the difference titration curves of Rollema et al. (1975) at 25 °C. Their conditions are not as close to ours as are those of the Antonini et al. (1965a) data, but the trend and magnitude of values are generally similar. The titration data of Antonini et al. (1965a) and of Rollema et al. (1975) are difficult to compare on an individual curve basis due to an

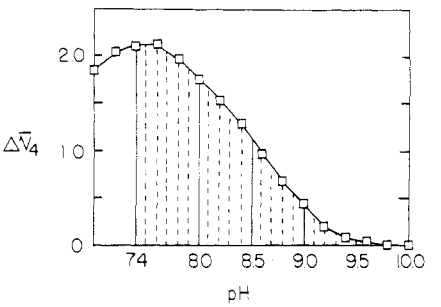

FIGURE 4: Integration of the difference titration data of Antonini et al. (1965a) to obtain free energies of the tetramer Bohr effect, $\delta\Delta G_{Bohr}$. $\Delta\bar{\nu}_4$ is the difference in the number of protons bound by unliganded and fully oxygenated forms of the protein. The stippled area below the curve is the integral of eq 16. Solid vertical lines denote integration limits corresponding to pH values of this study. Values are compared in Table V.

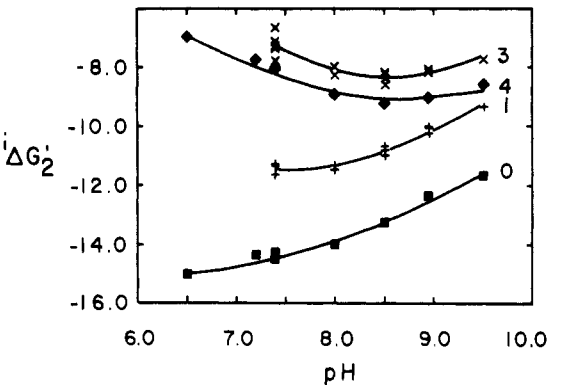

FIGURE 5: pH dependence of the subunit assembly free energy. Each curve and associated points represent a different state of oxygenation designated by the adjacent number. Quaternary enhancement is illustrated here by the lower stability of triply oxygenated tetramers relative to that of quadruply liganded species.

apparent difference in isoionic points for the hemoglobin preparations used.

(B) pH Dependence of Stepwise Parameters. (1) Free Energies of the Microscopic Reactions. Table III summarizes results of the multiparameter data-fitting process. From the best fit for each data set and pH, we calculated the intrinsic free energies of the successive tetramer oxygenation steps ($\Delta G'_{4i}$), i.e., corrected for statistical factors [cf. Mills et al. (1976)]. Also presented are the intrinsic dimer–tetramer assembly energies ($^{i}\Delta G'_2$) and the intrinsic intersubunit contact energies. Since the successive oxygenation energies for the middle two steps are less well resolved than their combined effect, values for their sum, $\Delta G'_{4(2+3)} = \Delta G'_{42} + \Delta G'_{43}$, are listed in Table III.

(2) Noncooperativity of Dimers. The possibility of cooperative oxygen binding by dimers was explored [cf. Mills et al. (1976) and Mills & Ackers (1979a)]. While acceptable confidence limits could not be obtained by floating $K_{coop\,2}$ as well as the other linkage parameters, the best-fit values scatter around unity for all pH values. Therefore, all parameter values reported in Table III were obtained with $K_{coop\,2} = 1.0$ and $^{0}K_2$ and $^{4}K_2$ held at their independently determined values for each pH.

(3) Energy States of the Tetramer. Relative to the noncooperative dimers, there are, at each pH, a minimum of four separate free-energy states of the tetramers: (1) unliganded; (2) singly liganded; (3) triply liganded; and (4) fully oxygenated species. This is shown in Figures 5–7 which illustrate the effects of ligation state on the resolved microscopic equilibrium constants. It is possible that a fifth state exists.

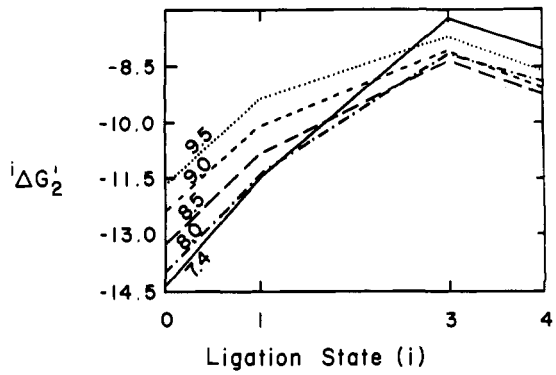

FIGURE 6: Effect of ligation state on stability of tetramers. $^{i}\Delta G'_2$ is the intrinsic free energy of dimer–tetramer assembly. The strength of the intersubunit interaction, as measured by $^{i}\Delta G'_2$, is seen to decrease progressively during the first three ligation steps, followed by an increase at the last step. This pattern is manifested at all pH values.

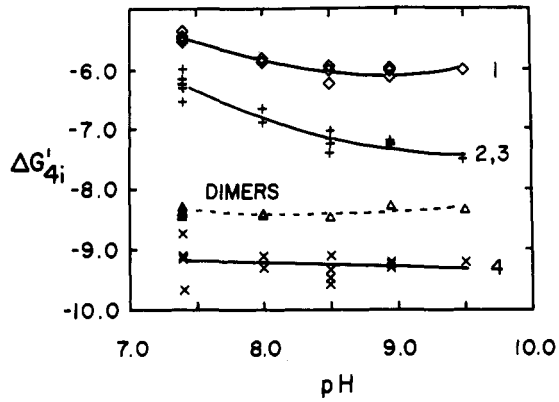

FIGURE 7: Stepwise free energies of oxygen binding. Intrinsic free energies, $\Delta G'_{4i}$, are given for the first and fourth binding steps and for the average of the middle two steps (2, 3). (---) Free energy per heme of oxygenating dissociated dimers. Quaternary enhancement is shown here as the higher affinity of tetramer binding at step 4 as compared with the dimeric affinity at the same pH.

However, we cannot resolve the assembly properties of doubly liganded tetramers with sufficient accuracy to assess this possibility.

If the linkage system is viewed in terms of a three-dimensional space in the three linked functions, Figures 5, 6, and 7 represent different projections in that space. Figure 5 shows the stepwise free energies of dimer–tetramer assembly as a function of pH. Figure 6 shows the distribution of these energies as a function of ligation state at each pH, and Figure 7 shows the stepwise oxygen binding energies as a function of pH. In the following sections, we describe various features of the results which are illustrated by these three figures.

(*4*) *Quaternary Enhancement.* In the first three stages of oxygenation, the binding of each oxygen "weakens" the subunit association at all pH values (Figures 5 and 6). By contrast, the binding of the fourth oxygen molecule considerably "strengthens" the association at every pH. To show that this is a statistically significant description of states, changes in $^{i}\Delta G_2$, the intersubunit contact energy, can be compared over the range of pHs (Table IIIB) along with their confidence limits. The term *quaternary enhancement* has been used to describe the increase in ligand binding affinity upon assembly of subunits (Mills & Ackers, 1979a). This is shown in Figure 7 as the higher affinity of the triliganded tetramer for oxygen ($\Delta G'_{44}$) compared with the dimers from which it is assembled.

Quaternary enhancement is thermodynamically linked to the progression of subunit assembly energies ($^{i}\Delta G'_2$) as the ligation state changes. This is shown in Figure 6. Similar effects were previously established over a range of temperatures

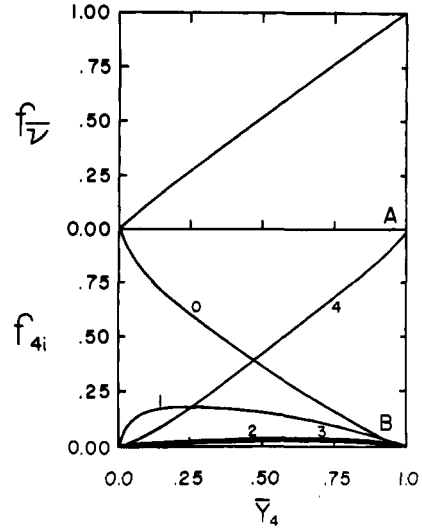

FIGURE 8: Overall proton release during saturation of tetramers with oxygen at pH 7.4. (A) Fraction $f_{\bar{\nu}}$ of the total Bohr effect as a function of $\bar{Y}$. (B) Population map of the various ligation states as a function of $\bar{Y}$.

at pH 7.4 (Mills & Ackers, 1979b).

(*5*) *pH Dependence of Cooperativity.* Substantial cooperativity in oxygen binding by the tetramer is seen at all pH values as the successive binding energies ($\Delta G'_{4i}$) increase 3–3.5 kcal between the first and last oxygens bound (Table IIIC). As noted above, none of the changes in cooperativity are attributable to variations in free energy at the last binding step. We also note that substantial cooperativity exists at pH 9.5 where the Bohr effect is absent.

(*6*) *Stepwise Bohr Effect in Tetramers.* Table IV gives the number of Bohr protons released per oxygen bound as a function of ligation state. Results for the second and third intermediate steps have been combined in this analysis. Figure 7 and Table IV show that the pH dependence of sequential oxygen binding falls into three categories. Over the pH range 7.4–8.5, 20–25% of the total Bohr protons are released at the first ligation step. The remaining fraction is released during the second and third steps, while the last oxygen molecule bound is not accompanied by significant release or absorption of protons. This partitioning of Bohr proton release is in accord with the measurements and predictions of Poyart et al. (1978). The unequal distribution of proton release is also consistent with the observed linearity of proton release with change in oxygen saturation (Antonini et al., 1963, 1965b; Olson & Gibson, 1973). Due to the cooperativity of oxygen binding, the predominant species in solution are unliganded and fully liganded tetramers as seen in Figure 8B. Plotting the fraction of total Bohr protons released by tetramers ($f_{\bar{\nu}}$) vs. fractional saturation ($\bar{Y}$) yields the curve in Figure 8A which has a maximum deviation from linearity of 2.5%.

(*C*) *Protons Released and Absorbed upon Assembly.* In addition to the assembly energies at intermediate ligation states ($^{1}\Delta G'_2$ and $^{3}\Delta G'_2$) as determined in the multiparameter analysis, the independently determined values of $^{0}\Delta G_2$ and $^{4}\Delta G_2$ have been analyzed for the number of protons associated with these reactions over the complete pH range. The pH dependence of these values and the second-order polynomial-fitted curves are shown in Figure 5. The corresponding numbers of protons are listed in Table IV. As in the temperature dependence study (Mills & Ackers, 1979b), trends in $^{1}\Delta G'_2$ are similar to those in $^{0}\Delta G_2$, and the relationship found between $^{3}\Delta G'_2$ and $^{4}\Delta G_2$ establishes quaternary enhancement. When values for $^{0}\Delta\bar{\nu}_2$, $^{4}\Delta\bar{\nu}_2$, $\Delta\bar{\nu}_4$, and $\Delta\bar{\nu}_2$ are summed, the total

number of protons absorbed or released around the linkage scheme is conserved by these estimates to within 0.05 proton at all pH values.

Discussion

The approach used in this study, and the previous ones of this series, differs entirely from that of nearly all hemoglobin oxygenation studies, which have been aimed solely at determining the tetrameric binding constants. Our primary focus of interest is upon the intersubunit interaction energies within the tetrameric molecule that change upon oxygenation. The use of subunit dissociation as a means of probing these interactions, as a function of oxygenation state, provides the most direct and reliable route to that information. In addition, the demonstration of self-consistency over the thermodynamic cycle of linkage scheme 1 using a variety of experimental techniques provides solid evidence that our oxygenation results are accurate. In the present investigation, the thermodynamic linkage between stepwise oxygen binding and subunit dissociation has been resolved at each of five pH values, encompassing most of the alkaline Bohr effect. The results have established the effects of protons on the oxygenation-linked intersubunit interaction energies and the changes in proton binding that accompany the detailed reaction steps of the linked system.

Certain aspects of our results can be compared with those of other experimental studies, including tetrameric oxygen binding measurements, tetrameric proton titration data, and results obtained previously by us on the oxygenation-linked dimer–tetramer assembly as a function of temperature.

(*A*) *Tetramer Bohr Effect.* The results we obtained for the total tetramer Bohr effect are in agreement with those of other studies (Antonini et al., 1965a; Rossi-Bernardi & Roughton, 1967; Rollema, 1975; Kilmartin & Rossi-Bernardi, 1969; Imai, 1979) as to the magnitude and pH dependence of proton release. As described earlier, our data are in close correspondence with those obtained by Antonini et al. (1965a).

The findings of this study in regard to the stepwise Bohr proton release are in general agreement with those of Imai (1979) in that we find unequal proton release for the four binding steps and very little proton release at the last step. This last feature is also in accord with inferences from the kinetic results of Noble and associates (McDonald & Noble, 1972; DeYoung et al., 1976; Kwiatkowski & Noble, 1982). Yassim & Fell (1982) have recently found a significant pH dependence of the last binding constant for hemoglobin within the red cell, where conditions are significantly different from those of this study.

(*B*) *Dimer Bohr Effect.* As described under Results, we find a thermodynamic correspondence between the proton titration results of Antonini et al. (1965a) and the pH-dependent oxygenation parameters of tetramers determined in this study. We are, therefore, able to calculate values of the dimeric Bohr effect by combining the dimer–tetramer equilibrium constants ${}^0K_2$ and ${}^4K_2$ (Chu & Ackers, 1981) with the tetramer proton titration numbers ${}^0\bar{\nu}_4$ and ${}^4\bar{\nu}_4$ (Antonini et al., 1965a) in order to estimate ${}^0\bar{\nu}_2$ and ${}^2\bar{\nu}_2$ (and the difference $\Delta\bar{\nu}_2$) according to eq 23. The results of this calculation are shown in Table VI where the estimated difference $\Delta\bar{\nu}_2$ in dimer-bound protons brought about by oxygenation is compared with the values obtained by using eq 20. It can be seen from Table VI that the two determinations, based on different combinations of experimental information, are in good agreement with regard to the magnitude of the effect and the trend with pH. These results provide further support for the existence of the dimer Bohr effect. This effect is similar in magnitude to the Bohr

Table VI: Estimation of Dimer Bohr Effect

pH	$\Delta\bar{\nu}_2$ from eq 23	$\Delta\bar{\nu}_2$ from eq 20
9.0	+0.28	+0.16 ± 0.09
8.8	+0.19	
8.6	+0.08	
8.5		+0.05 ± 0.04
8.4	−0.04	
8.2	−0.13	
8.0	−0.23	−0.07 ± 0.05
7.8	−0.30	
7.6	−0.33	
7.4	−0.31	−0.22 ± 0.12

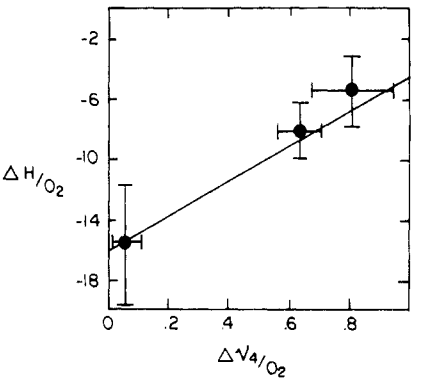

FIGURE 9: Correlation of stepwise oxygen binding enthalpies, ΔH_i, with stepwise Bohr proton release, $\Delta\bar{\nu}_{4i}$, for tetramers.

effect found in isolated subunit chains (Rollema et al., 1976). We surmise that the dimer Bohr effect corresponds to that component of the tetramer Bohr effect which is contributed by the tertiary structure changes that accompany ligation of the various subunits. The total Bohr effect for the tetramer must also include the proton release resulting from quaternary structure change.

(*C*) *Stepwise Correlation of Bohr Proton Release with Enthalpic Changes.* In previous studies, a striking correspondence was observed between the overall heat of Bohr proton release for tetramers and the reduction in the enthalpy of oxygen binding which results from subunit assembly (Mills et al., 1979; Mills & Ackers, 1979b; Ackers, 1980). This, and related observations, suggested that the enthalpic contribution to the free energy of cooperativity in oxygen binding by tetramers may be accounted for entirely by the heat of Bohr proton release; i.e., the observed enthalpy of fully oxygenating tetramers, ΔH_{obsd}, can be described by the relationship

$$\Delta H_{obsd} = \Delta H_{int} + \Delta\bar{\nu}_4\Delta H_{H^+} \qquad (25)$$

where ΔH_{int} is the intrinsic enthalpy of oxygenation observed for isolated chains and dimers, $\Delta\bar{\nu}_4$ is the number of moles of Bohr protons released, and ΔH_{H^+} is the enthalpy change that accompanies the release of a mole of Bohr protons. A question of great interest then is whether a relationship like eq 25 can be satisfied at each step of oxygenation.

The distribution of stepwise proton release found in this study provides a strong correlation between the heat of proton release and the stepwise enthalpies of oxygen binding. The enthalpy of binding oxygen for the first three steps is reduced in magnitude from that found in isolated chains or dimers. Figure 9 shows the enthalpies per oxygen bound for successive steps plotted against the corresponding number of protons released. These enthalpies were obtained through van't Hoff analysis of the temperature dependence of stepwise free energies (Mills & Ackers, 1979b) combined with the pH 7.4, 21.5 °C set obtained in this study [ΔH_{41} = 8.1 ± 1.8 kcal/mol of O_2, $(\Delta H_{42} + \Delta H_{43})/2$ = −5.5 ± 2.2 kcal/mol of O_2, ΔH_{44}

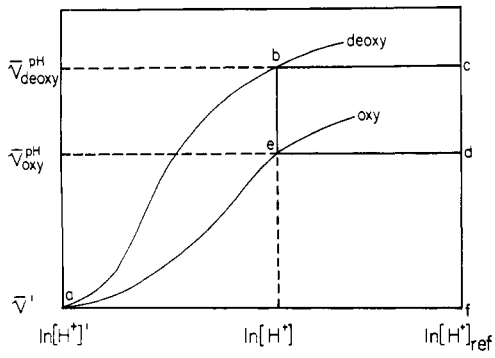

FIGURE 10: Hypothetical acid–base titration curves for unliganded and fully oxygenated hemoglobin tetramers, illustrating the chemical work of proton binding.

= −15.7 ± 4.3 kcal/mol of O_2]. The solid line is an independent prediction based on the overall enthalpy of the Bohr effect: ΔH_{4^+} = 11 kcal/mol of proton released (Antonini et al., 1965a; Chipperfield et al., 1967). It is obvious that, to within determinable confidence limits, the Bohr proton release may account for all of the reduction in enthalpy associated with the cooperativity of oxygen binding.

(*D*) *Quaternary Enhancement Effect.* The magnitude of the quaternary enhancement effect in normal hemoglobin is found to be independent of both pH (as found in this study) and temperature (Mills & Ackers, 1979). It thus appears to be an entropic effect not linked to significant proton binding reactions. The basis of this effect in hemoglobin appears to depend on the relation between tertiary states of subunits and quaternary states of the tetrameric structure in which they exist. Isolated β chains bind oxygen or carbon monoxide with an increased affinity when assembled into the tetrameric structure (Valdes & Ackers, 1977a,b). The β_4 tetramer, whether unliganded or liganded, bears a close resemblance in quaternary structure to that of liganded normal hemoglobin (Arnone et al., 1982; A. Arnone, unpublished results). Moreover, the magnitude of the quaternary enhancement free energy per heme in β chains is nearly identical with that of normal hemoglobin. These findings suggest that the origin of quaternary enhancement may be an unfavorable free energy contribution that arises when an unligated subunit is present in an "oxy" quaternary structure. Similarly, we might expect an unfavorable free energy contribution when a ligated subunit is present in a "deoxy" quaternary structure.

(*E*) *Concluding Remarks.* Apart from their relevance to the problem of hemoglobin function, these results are unique in that no other linkage system of comparable complexity has been solved at this level of detail. The hemoglobin system was resolved in this study into a basic set of 35 independent thermodynamic parameters, from which the remaining ones were derived. These results are in turn only part of a much more extensive linkage system for which self-consistent information is presently available. This system includes the temperature dependence studies of normal hemoglobin at pH 7.4 (Mills & Ackers, 1979b), the studies on subunit chains (Mills et al., 1979; Valdes & Ackers, 1977a,b), the detailed linkage studies on the variant hemoglobin Kansas (Atha & Riggs, 1975; Atha et al., 1979), and the recent studies on 22 mutant and chemically modified hemoglobins for which $^0K_2$ and $^4K_2$ have been determined (Pettigrew et al., 1982). The extensive base of accurate data that has been generated (e.g., see supplementary material) and the thermodynamic results derived from these data should be useful in future studies for critically testing and formulating mechanistic theories and models of hemoglobin function. In subsequent papers, we will present such analyses. We are currently extending the model-independent thermodynamic studies to incorporate the effects of organic phosphate on the oxygenation-linked dimer–tetramer assembly system.

Acknowledgments

This paper is dedicated to the memory of Eraldo Antonini, whose scientific work and personal demeanor were an inspiration to all of us who knew him.

Supplementary Material Available

Tabulations of oxygenation data sets (106 pages). Ordering information is given on any current masthead page.

Appendix

(*A*) *Chemical Work of Proton Binding.* Figure 10 shows diagrammatically two acid–base titration curves, hypothetically for unliganded (deoxy) and fully oxygenated (oxy) hemoglobin tetramers. At some proton concentration $[H^+]'$, the curves coincide (point a), and the degree of saturation is $\bar{\nu}'$. Consider the chemical work of loading one of the species, e.g., deoxyhemoglobin, with protons. Protons are brought (hypothetically) from a reservoir at the standard-state chemical potential ($\mu°$) corresponding to the proton activity $[H^+]_{ref}$ to a pH where the chemical potential is $\mu = \mu^0 + RT \ln [H^+]$. For simplicity, consider $[H^+]_{ref}$ to be the unit activity of protons. The work of transferring an increment $d\bar{\nu}$ of protons and adding it to the protein is $(\mu - \mu°)d\bar{\nu} = RT \ln ([H^+])d\bar{\nu}$. Now if this loading process is carried out over the range of saturation between $\bar{\nu}'$ and the value $\bar{\nu}_{deoxy}$ corresponding to $\ln [H^+]$, the free energy ΔG_{deoxy} of the process is given by the integral

$$\Delta G_{deoxy} = RT \int_{\bar{\nu}'}^{\bar{\nu}_{deoxy}{}^{pH}} \ln [H^+]\, d\bar{\nu}_{deoxy} = \text{area}(abcfa)RT$$

Similarly, when the oxygenated molecule is loaded with protons up to the same pH, the free energy ΔG_{oxy} will be given by

$$\Delta G_{oxy} = RT \int_{\bar{\nu}'}^{\bar{\nu}_{oxy}{}^{pH}} \ln [H^+]\, d\bar{\nu}_{oxy} = \text{area}(aedfa)RT$$

Integrating by parts the right side of each expression, and subtracting, we have

$$\Delta G_{deoxy} - \Delta G_{oxy} = -RT \int_{[H^+]'}^{[H^+]} (\bar{\nu}_{deoxy} - \bar{\nu}_{oxy})\, d \ln [H^+] + RT \ln ([H^+])\left(\bar{\nu}^{H^+}_{deoxy} - \bar{\nu}^{H^+}_{oxy}\right)$$

The last term on the right is the work of transferring $\bar{\nu}_{deoxy} - \bar{\nu}_{oxy}$ moles of protons from the reference-state reservoir to the reaction system at proton activity $[H^+]$ and is equal to the rectangle $(bcdeb)RT$. The remaining term, therefore, is the difference in chemical work of proton binding when the activity is raised from $[H^+]'$ to $[H^+]$.

Therefore, we have

$$\Delta G^{H^+}_{oxy} - \Delta G^{H^+}_{deoxy} = RT \int_{[H^+]'}^{[H^+]} (\bar{\nu}_{oxy} - \bar{\nu}_{deoxy})\, d \ln [H^+]$$

which is identical with eq 16.

(*B*) *Mathematical Symbols Used in Equations and Formulas*:

K_{2i}, equilibrium constant for binding i oxygen molecules onto a dimer (i = 1, 2)

k_{2i}, equilibrium constant for binding the ith oxygen molecule onto a dimer (i = 1, 2)

K_{4i}, equilibrium constant for binding i oxygen molecules onto a tetramer (i = 1, 2, 3, 4)

k_{4i}, equilibrium constant for binding the ith oxygen molecule onto a tetramer (i = 1, 2, 3, 4)

k'_{2i} and k'_{4i}, equilibrium constants k_{2i} and k_{4i} corrected for statistical factors

ΔG_{2i} and ΔG_{4i}, Gibbs free energies corresponding to k_{2i} and k_{4i}, respectively
$\Delta G'_{2i}$ and $\Delta G'_{4i}$, free energies corresponding to k'_{2i} and k'_{4i}, respectively
ΔG_2, free energy of binding two oxygens onto a dimer
ΔG_4, free energy of binding four oxygens onto a tetramer
${}^iK_2$, equilibrium constant for assembly of a tetramer with i ligands bound from two dimers as shown in linkage scheme 1
${}^iK_2{}^0$, dimer–tetramer assembly equilibrium constant for a tetramer with i oxygens, but no protons, bound
${}^i\Delta G_2$, free energy corresponding to ${}^iK_2$
${}^i\Delta G'_2$, free energy corresponding to ${}^iK_2$ after correction for statistical factor
$\bar{Y}$, total fractional saturation with oxygen for all hemoglobin species
$\bar{Y}_2$, fractional saturation of dimers with oxygen
$\bar{Y}_4$, fractional saturation of tetramers with oxygen
$[P_t]$, total concentration of hemoglobin (molar heme)
[X], molar concentration of unbound oxygen in solution
$[\bar{X}]$, median oxygen concentration
f_2, fraction of hemoglobin present in dimeric form regardless of oxygenation state
f_4, fraction of hemoglobin present in tetrameric form regardless of oxygenation state
f_{4i}, fraction of hemoglobin present as tetramers with i oxygens bound
$f_{\bar{\nu}}$, fraction of the tetramer Bohr effect
${}^0f_2$, fraction of unliganded hemoglobin present as dimers
${}^4f_2$, fraction of fully oxygenated hemoglobin present as dimers
Z_2, binding polynomial for dimers binding oxygen
Z_4, binding polynomial for tetramers binding oxygen
$Z_2^{H^+}$, binding polynomial for dimers binding protons
$Z_4^{H^+}$, binding polynomial for tetramers binding protons
$Z_{oxy}^{H^+}$, binding polynomial for binding protons by fully oxygenated tetramers
$Z_{deoxy}^{H^+}$, binding polynomial for binding protons by deoxygenated tetramers
$\Delta G_{deoxy}^{H^+}$, free energy of protonation for deoxygenated tetramers
$\Delta G_{oxy}^{H^+}$, free energy of protonation for fully oxygenated tetramers
$\Delta G_4^{\bar{\nu}'}$, free energy of oxygenation for tetramers at proton saturation $\bar{\nu}'$
$\delta\Delta G_{Bohr}$, linkage free energy of the Bohr effect
$[H^+]$, activity of unbound protons in solution
$\bar{\nu}_{oxy}$, fractional saturation with protons for oxygenated tetramers
$\bar{\nu}_{deoxy}$, fractional saturation with protons for deoxygenated tetramers
$\Delta\bar{\nu}_4$, number of protons released upon complete oxygenation of tetramers (total tetrameric Bohr effect)
$\Delta\bar{\nu}_2$, number of protons released upon complete oxygenation of dimers (total dimeric Bohr effect)
${}^i\Delta\bar{\nu}_2$, number of protons bound upon assembly of a tetramer with i oxygens bound from the appropriate combination of dimers
${}^i\bar{\nu}_2$, fractional saturation with protons for hemoglobin dimers with i oxygens bound
${}^i\bar{\nu}_4$, fractional saturation with protons for hemoglobin tetramers with i oxygens bound
$K_{44}{}^0$, equilibrium constant for binding four oxygens onto a tetramer when no protons are bound
$K_{coop\,2}$, measure of cooperativity in oxygenation of dimers, equal to $K_{21}/[2(K_{22})^{1/2}]$
ΔH_{obsd}, observed enthalpy of oxygenation for tetramers
ΔH_{int}, intrinsic enthalpy of oxygenation for tetramers
ΔH_{H^+}, enthalpy of releasing 1 mol of protons upon oxygenation of tetramers
k_t^{oxy} and k_t^{deoxy}, equilibrium constant for binding t protons to oxygenated and deoxygenated tetramers, respectively
μ, chemical potential for protons at activity $[H^+]$
μ°, standard-state chemical potential for protons

Registry No. O_2, 7782-44-7; hydrogen ion, 12408-02-5; Hb A_0, 54651-57-9.

References

Ackers, G. K. (1976) *Proteins (3rd Ed.) 1*, 1.
Ackers, G. K. (1980) *Biophys. J. 32*, 331–346.
Ackers, G. K., & Halvorson, H. R. (1974) *Proc. Natl. Acad. Sci. U.S.A. 91*, 4312–4316.
Ackers, G. K., & Johnson, M. L. (1981) *J. Mol. Biol. 147*, 559–582.
Ames, B. N., & Dubin, D. T. (1960) *J. Biol. Chem. 235*, 769–775.
Antonini, E., Wyman, J., Brunori, M., Bucci, E., Fronticelli, C., & Rossi-Fanelli, A. (1963) *J. Biol. Chem. 238*, 2950–2957.
Antonini, E., Wyman, J., Brunori, M., Fronticelli, C., Bucci, E., & Rossi-Fanelli, A. (1965a) *J. Biol. Chem. 240*, 1096–1103.
Antonini, E., Schuster, T., Brunori, M., & Wyman, J. (1965b) *J. Biol. Chem. 240*, 2262–2264.
Arnone, A., Briley, P. D., Rogers, P. H., & Henrickson, W. A. (1982) in *Interaction between Iron and Protein and Oxygen and Electron Transport* (Chien, H., Ed.) pp 127–133, Elsevier/North-Holland, New York.
Atha, D. H., & Riggs, A. (1976) *J. Biol. Chem. 251*, 5537–5543.
Atha, D. H., Johnson, M. L., & Riggs, A. (1979) *J. Biol. Chem. 254*, 12390–12398.
Chipperfield, J. R., Rossi-Bernardi, L., & Roughton, F. J. W. (1967) *J. Biol. Chem. 242*, 777–783.
Chu, A. H., & Ackers, G. K. (1981) *J. Biol. Chem. 256*, 1199–1205.
DeYoung, A., Pennelly, R. R., Tan-Wilson, A. L., & Noble, R. W. (1976) *J. Biol. Chem. 251*, 6692–6698.
Edsall, J. T. (1972) *J. Hist. Biol. 5*, 205–257.
El-Yassim, D. I., & Fell, D. A. (1982) *J. Mol. Biol.* 863–889.
Evelyn, K. A., & Malloy, H. T. (1938) *J. Biol. Chem. 126*, 655–662.
Flanagan, M. A., Ackers, G. K., Hanania, G. I. H., & Gurd, F. R. N. (1981) *Biochemistry 20*, 7439–7449.
Haupt, G. W. (1952) *J. Opt. Soc. Am. 42*, 441–447.
Hayashi, A., Suzuki, T., & Shin, M. (1973) *Biochim. Biophys. Acta 310*, 310–316.
Imai, K. (1973) *Biochemistry 12*, 798–808.
Imai, K. (1979) *J. Mol. Biol. 133*, 233–247.
Imai, K. (1981) *Methods Enzymol. 76*, 470–488.
Imai, K., & Yonetani, T. (1975) *J. Biol. Chem. 250*, 7093–7098.
Imai, K., Morimoto, H., Kotani, M., Watari, H., Waka, H., & Kuroda, M. (1970) *Biochim. Biophys. Acta 200*, 189–196.
Ip, S. H. C., & Ackers, G. K. (1977) *J. Biol. Chem. 252*, 82–87.
Ip, S. H. C., Johnson, M. L., & Ackers, G. K. (1976) *Biochemistry 15*, 654–660.
Johnson, M. L., & Ackers, G. K. (1977) *Biophys. Chem. 7*, 77–80.
Johnson, M. L., & Ackers, G. K. (1982) *Biochemistry 21*, 201–211.

Johnson, M. L., Halvorson, H. R., & Ackers, G. K. (1976) *Biochemistry 15*, 5363-5371.
Johnson, M. L., Turner, B. W., & Ackers, G. K. (1984) *Proc. Natl. Acad. Sci. U.S.A.* (in press).
Kilmartin, J. V., Fogg, J. H., & Perutz, M. F. (1980) *Biochemistry 19*, 3189-3193.
Kwiatkowski, L. D., & Noble, R. W. (1982) *J. Biol. Chem. 257*, 8891-8895.
Makino, J., & Sugita, Y. (1982) *J. Biol. Chem. 257*, 163-168.
Matthew, J. B., Hanania, G. I. H., & Gurd, F. R. N. (1979a) *Biochemistry 18*, 1919-1927.
Matthew, J. B., Hanania, G. I. H., & Gurd, F. R. N. (1979b) *Biochemistry 18*, 1928-1935.
McDonald, M. J., & Noble, R. W. (1972) *J. Biol. Chem. 247*, 4282-4287.
Mills, F. C., & Ackers, G. K. (1979a) *Proc. Natl. Acad. Sci. U.S.A. 76*, 273-277.
Mills, F. C., & Ackers, G. K. (1979b) *J. Biol. Chem. 254*, 2881-2887.
Mills, F. C., Johnson, M. L., & Ackers, G. K. (1976) *Biochemistry 15*, 5350-5362.
Mills, F. C., Ackers, G. K., Gaud, H., & Gill, S. J. (1979) *J. Biol. Chem. 254*, 2875-2880.
Olson, J., & Gibson, Q. (1973) *J. Biol. Chem. 248*, 1623-1630.
Pettigrew, D. W., Romeo, P. H., Tsapis, A., Thillet, J., Smith, M. L., Turner, B. W., & Ackers, G. K. (1982) *Proc. Natl. Acad. Sci. U.S.A. 79*, 1849-1853.
Poyart, C., Bursaux, E., & Bohn, B. (1978) *Eur. J. Biochem. 87*, 75-83.
Rollema, H. S., deBruin, S. H., Janssen, L. H. M., & van Os, G. A. J. (1975) *J. Biol. Chem. 250*, 1333-1339.
Rollema, H. S., deBruin, S. H., & van Os, G. A. J. (1976) *FEBS Lett. 51*, 148-150.
Rossi-Bernardi, L., & Roughton, F. J. W. (1967) *J. Biol. Chem. 242*, 784-792.
Russu, I. M., Ho, N. T., & Ho, C. (1982) *Biochemistry 21*, 5031-5043.
Smith, F. R., & Ackers, G. K. (1983) *Biophys. J. 41*, 415.
Szabo, A., & Karplus, M. (1972) *J. Mol. Biol. 72*, 163-197.
Turner, B. W., Pettigrew, D. W., & Ackers, G. K. (1981) *Methods Enzymol. 76*, 596-628.
Valdes, R., & Ackers, G. K. (1977a) *J. Mol. Biol. 252*, 74-81.
Valdes, R., & Ackers, G. K. (1977b) *J. Biol. Chem. 252*, 88-91.
Valdes, R., & Ackers, G. K. (1978a) *Proc. Natl. Acad. Sci. U.S.A. 75*, 311-314.
Valdes, R., & Ackers, G. K. (1978b) in *Biochemical and Clinical Aspects of Hemoglobin Abnormalities* (Caughey, W. S., Ed.) pp 527-532, Academic Press, New York.
van Assendelft, O. W., & Zijlstra, W. G. (1975) *Anal. Biochem. 69*, 43-48.
Williams, R. C., Jr., & Tsay, K. Y. (1973) *Anal. Biochem. 54*, 137-145.
Wyman, J. (1964) *Adv. Protein Chem. 18*, 223-285.

Structure of the Carboxyl Propeptide of Chicken Type II Procollagen Determined by DNA and Protein Sequence Analysis†

Yoshifumi Ninomiya, Allan M. Showalter, Michel van der Rest, Nabil G. Seidah, Michel Chrêtien, and Bjorn R. Olsen*

ABSTRACT: The complete amino acid sequence of the carboxyl propeptide of chicken type II procollagen has been determined by nucleotide sequencing of three recombinant plasmids harboring inserts complementary to type II collagen messenger RNA (mRNA). In addition, we have characterized a recombinant plasmid containing sequences from the 3'-nontranslated region of type II collagen mRNA. Since the nucleotide sequences did not correspond to regions of chicken type II procollagen for which protein sequence data exist, we have also purified the physiologically cleaved type II carboxyl propeptide from organ cultures of chick embryo sternal cartilages and determined its amino-terminal amino acid sequence by automated Edman degradation. A comparison of the nucleotide-derived sequence with the sequence obtained by Edman degradation of the type II carboxyl propeptide provides definitive proof that the recombinant plasmids contain sequences specific for type II procollagen and allows for the elucidation of the cleavage site for procollagen C-protease within type II procollagen. The results of our sequence analysis indicate that the type II carboxyl propeptide contains 246 amino acid residues. When the peptide is compared with the homologous region of pro α1(I) chains, the type II carboxyl propeptide appears to have an inserted amino acid residue in position 7 (counted from the C-protease cleavage site) and a deleted amino acid residue at position 101. The type II carboxyl propeptide is similar to that of pro α1(I) chains in that it contains eight cysteinyl residues in the same positions, but it is different from the pro α1(I) peptide in that it contains two potential sites for N-linked oligosaccharide side chains while the pro α1(I) peptide contains only one such site.

The collagens are members of a class of structural proteins that are encoded by at least 10 gene loci [for a review, see Bornstein & Sage (1980)]. The modulated expression of these different loci appears to be crucial in normal embryonic development and in tissue repair processes. Isolation of different collagen genes and studies on their regulation are therefore of considerable interest.

The major collagen genes expressed by fibroblasts and osteoblasts are those of type I collagen. This collagen type contains triple-helical molecules composed of two α1(I) chains and one α2(I) chain, and it represents the major collagen type in skin, tendon, ligaments, and bone. In contrast, normal

† From the Department of Biochemistry, UMDNJ-Rutgers Medical School, Piscataway, New Jersey 08854 (Y.N., A.M.S., and B.R.O.), the Genetics Unit, Shriners Hospital, Montreal, Canada H3G 1A6 (M.v.d.R.), and the Clinical Research Institute of Montreal, Canada H2W 1R7 (N.G.S. and M.C.). *Received July 26, 1983.* This study was supported by Research Grant AM 21471 from the National Institutes of Health and by a Johnson & Johnson graduate student fellowship (to A.M.S.).

0006-2960/84/0423-0617$01.50/0